Ligand-induced global transitions in the catalytic domain of protein kinase A

Changbong Hyeon[a], Patricia A. Jennings[b], Joseph A. Adams[c], and José N. Onuchic[d,1]

[a]Department of Chemistry, Chung-Ang University, Seoul 156-756, Republic of Korea; and Departments of [b]Chemistry and Biochemistry and [c]Pharmacology and [d]Center for Theoretical Biological Physics and Department of Physics, University of California at San Diego, La Jolla, CA 92093

Contributed by José N. Onuchic, December 30, 2008 (sent for review December 6, 2008)

Conformational transitions play a central role in the phosphorylation mechanisms of protein kinase. To understand the nature of these transitions, we investigated the dynamics of nucleotide binding to the catalytic domain of PKA, a prototype for the protein kinase enzyme family. The open-to-closed transition in PKA was constructed as a function of ATP association by using available X-ray data and Brownian dynamics. Analyzing the multiple kinetic trajectories at the residue level, we find that the spatial rearrangement of the residues around the nucleotide-binding pocket, along with suppressed local fluctuations, controls the compaction of the entire molecule. In addition, to accommodate the stresses induced by ATP binding at the early transition stage, partial unfoldings (cracking) and reformations of several native contacts occur at the interfaces between the secondary structure motifs enveloping the binding pocket. This suggests that the enzyme experiences local structural deformations while reaching its functional, ATP-bound state. Our dynamical view of the ligand-induced transitions in PKA suggests that the kinetic hierarchy of local and global dynamics, the variable fluctuation of residues and the necessity of partial local unfolding may be fundamental components in other large scale allosteric transitions.

allostery | cracking | fragility | kinetic hierarchy | open-to-closed transitions

The ability of enzymes to transform enzyme–substrate contacts into catalytic power allows otherwise inert chemical processes to proceed in the reasonable time frame for the cell. Discovering the detailed mechanism of the catalytic process has been the goal of enzymologists for many decades. We have learned that the active site appears well adapted to the transition state structure as originally proposed by Pauling (1) and that many chemical factors such as enzyme-linked intermediates, metal cofactors, and vitamin-based coenzymes actively participate in lowering the energy barrier to product formation. The idea that the structural dynamics of enzymes can also participate in these chemical transformations is now accepted as a possible additional mechanism. In recent years, methods to probe these dynamics have grown enormously (2–4). Many enzymes can be crystallized in more than one structural conformation, raising the possibility that the structures with lowered energy barrier may be directly associated with the conversion of substrate to product. Diverse solution methods (5–8) have also shown that specific regions within the enzyme are in dynamic flux and that the binding of ligands can significantly modify the dynamics in unique ways (9–11). Although these phenomena are likely to be critical for catalysis, a significant dilemma facing structural biology is to correlate experimentally obtained "frozen" structures with a quantitative understanding of the functional mechanism. Much data now point to the high flexibility of enzymes in both crystalline and solution forms, but the linkage between these soft aspects of enzymes and the harder catalytic steps is poorly understood.

Since the first observations by Krebs and Fischer (12), the knowledge of protein phosphorylation has blossomed from a curious mechanism for the regulation of sugar metabolism to a widespread posttranslational modification. The addition of 1 or more phosphates to hydroxyl-bearing amino acids is catalyzed by protein kinases, a large family of enzymes that all share a well-conserved catalytic core of ≈250 residues (13). Despite the simplicity of the reaction catalyzed by these enzymes, the protein kinases are regulated in complex ways that may involve phosphorylation by other kinases (14), membrane and organelle localization through scaffolding proteins (15), and protein–protein and domain–domain interactions through regulator modules (16, 17). In the last decade, a full appreciation for the conformational complexity of these enzymes has been developed (11, 18). The essential kinase core has been crystallized in many different conformations (19–21) that are distinguished by rotations between the ATP and substrate-binding lobes and by movements in various secondary structural elements. These properties have become very important to investigate on practical grounds because many known inhibitors can induce different conformational states in the enzymes that are important for inhibitor design. Given the general importance of the protein kinases and their role in disease, such induced-fit changes (22), which may be accompanied by partial unfolding (cracking) (23–25), are important to understand not only from a regulatory perspective but also from a drug therapy approach.

One protein kinase that has served as a prototype for this enzyme family is the catalytic subunit of cAMP-dependent protein kinase (PKA). PKA is activated by phosphorylation in its activation loop (Thr-197) and, conversely, repressed by the binding of a regulatory subunit. Based on X-ray diffraction studies, these regulatory functions have been connected to the conformational changes of PKA. In addition to these modulators, H–D exchange and proteolytic cleavage studies have shown that ATP binding and reaction product ADP can induce the changes in the solution structure of PKA (2, 9). Interestingly, nucleotide binding results in conformational changes in regions far outside the active site in the C-terminal tail and helix C, suggesting that the kinase core may experience a modal conductance of conformational flux in only specific regions or channels of the core. This example of nucleotide-induced changes in conformation is particularly relevant to catalysis because it has been demonstrated that ADP release is the rate-limiting step in catalysis for PKA (26, 27). Such observations raise the exciting possibility that conformational changes in PKA may be coupled to an event that governs the net rate of protein phosphorylation. These early studies, however, lack a useful correlation between observed conformational changes, such as those observed in H–D exchange experiments (2) and the 3-dimensional structure of the enzyme (21).

Toward the next level of understanding, we have computationally investigated the ATP-binding induced PKA dynamics by using the open and closed forms of crystal structures. A direct comparison between the 2 structures suggests that the space of the binding cleft

Author contributions: C.H., P.A.J., and J.N.O. designed research; C.H. performed research; C.H., P.A.J., J.A.A., and J.N.O. analyzed data; and C.H., P.A.J., J.A.A., and J.N.O. wrote the paper.

The authors declare no conflict of interest.

[1]To whom correspondence should be addressed at: Center for Theoretical Biological Physics, University of California at San Diego, 9500 Gilman Drive, La Jolla, CA 92093-0374. E-mail: jonuchic@ucsd.edu.

This article contains supporting information online at www.pnas.org/cgi/content/full/0813266106/DCSupplemental.

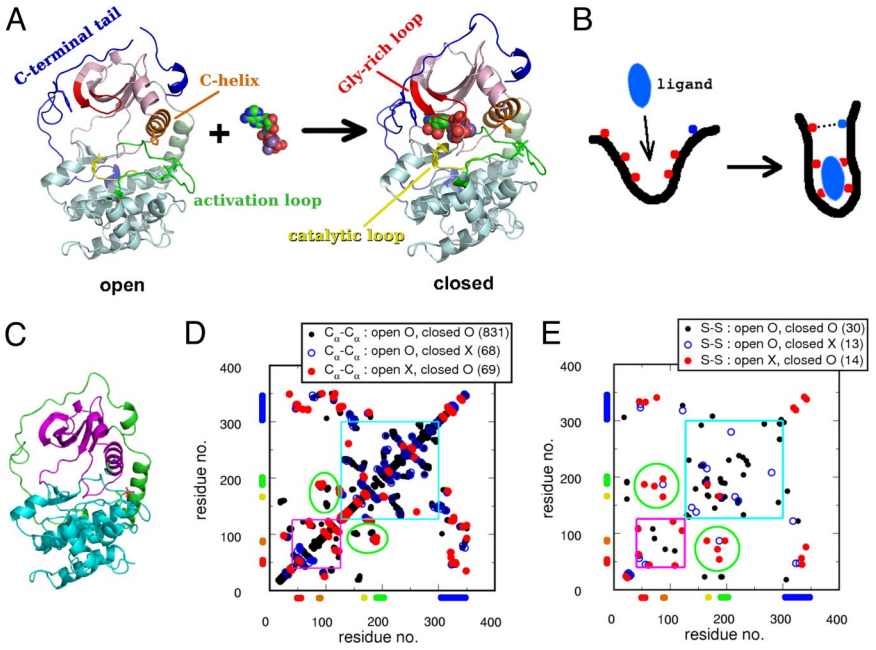

Fig. 1. Modeling PKA transitions. (*A*) Open-to-closed transitions of PKA induced by ATP. The key regions of Gly-rich loop (residues 47–58), C-helix (residues 85–97), catalytic loop (residues 166–171), activation loop (residues 184–204), and C-terminal tail (residues 301–350) are colored in red, orange, yellow, green, and blue, respectively. (*B*) An illustration of ligand-induced transitions. In this cartoon, the balls in red and blue attract, but the balls of the same color repel each other. The insertion of ligand (blue ellipse) into the binding pocket compacts the whole system by making contacts with red balls. An additional contact between the red and blue balls at the ends of the chain is made in the presence of ligand in its binding pocket, further compacting the whole system. This basic idea is employed in modeling the PKA transition dynamics coupled with an ATP. (*C*) Small lobe, large lobe, and the rest of the structure are colored in purple, cyan, and green, respectively. (*D*) Native contact maps for backbone with a contact cutoff, $R_c^B = 8$ Å. (*E*) Native contact maps for side chains with $R_c^S = 5$ Å. In *D* and *E*, the native contacts analyzed from open (PDB ID code 1CMK) and closed (PDB ID code 1ATP) structures are shown. The total number of contacts is specified inside the parentheses in the boxes above the images. The contacts enclosed in the purple and cyan boxes are the ones within the small and large lobes, respectively. The interlobe contacts are enclosed in green circles.

is reduced upon ATP binding (Fig. 1*A*). Although the structural difference measured by the C_α backbone RMSD is only $\lesssim$1.3 Å, the conformational adaptation of the PKA to the ATP, recapitulated as the "induced fit mechanism" (22), is well manifested in this system. Therefore, one can gain several microscopic insights from this system by analyzing the transition dynamics at the residue level. To simulate PKA conformational change, (*i*) we model PKA structure by using an energy Hamiltonian stabilizing the open structure as a basis of interaction potential. (*ii*) Next, we explicitly take into account the intermolecular contacts between the PKA and ATP, so that the local compaction of PKA is achieved upon the ATP binding. Our simulations show that PKA remains in the open conformation in the absence of ATP and is transformed into the closed conformation upon ATP binding. Although ATP interactions alone are sufficient to qualitatively observe global transitions, additional native contacts from the closed state is required to achieve the complete conversion toward the closed structure. [see supporting information (SI) *Text* for the details]. There are relatively few computational studies on the transition dynamics of kinases, which includes adenylate (28–3), c-Src (32, 33), Abl (34), and cyclin-dependent kinase 5 (CDK5) (35). Most interpretations on conformational dynamics rely on equilibrium free-energy surfaces calculated from sampling procedures (28, 29, 32–35) or on the results from short-time all-atom molecular dynamics (31, 34, 35). Our in-depth study on PKA dynamics is unique in that multiple trajectories of full open-to-closed transition dynamics are studied in real time with an explicitly modeled ATP ligand. Our simulation and analysis mimic the style of recent single-molecule experiments that provide tools to decipher the real-time dynamics of protein by tracking the "distance" between tagged residues (3, 4). Statistical analysis on the PKA dynamics is made at both global and local levels, unraveling the complexity of the transition dynamics.

Results and Discussion

Overview of PKA Structure and Dynamics. The PKA structure consisting of 350 residues is divided into the small (residues 41–126) and large (residues 127–300) lobes and the N-(residues 1–40) and C-(residue 301–350) terminal tails. The binding cleft for ATP is surrounded by the glycine (Gly)-rich loop (Gly lid, residues 47–58) and the catalytic loop (residues 166–171) composed of several charged residues (see Fig. 1*A* and Fig. S1). The insertion of ATP compacts the binding cleft, stabilizing the interlobe contacts (see Fig. 1 *B*, *D*, and *E*) between the Mg^{2+} binding loop and activation loop (residues 184–204) (36). ATP binding causes a clockwise rotation of the C-terminal tail, allowing Phe-327 to contact ATP (2), which further enhances the compaction between the small and large lobes.

Analysis of Simulated Trajectories. To quantitatively monitor the dynamics, we measure the interresidue distances (see Fig. 2*A*). Three pairs of distance reporters (21) are used for probing the PKA dynamics (to identify the position of a residue in sequence space, see Fig. 1 *D* and *E*): (*i*) The Ser-53/Gly-186 pair measures the motion of the Gly-rich loop relative to the Mg^{2+} positioning loop (residues 184–187). This should be sufficient to detect the ATP in the binding cleft. (*ii*) The His-87/P-Thr-197 pair monitors the distance between the C-helix and activation loop. The activation loop in PKA is stabilized by the phosphorylation of Thr-197, a posttranslational modification that is essential for optimal activity (37–41). The crystal structure of the closed form suggests that the hydrogen bond between His-87 and P-Thr-197 is a key element for this stabilization/activation. The P-Thr-197 also mediates repulsion between Arg-165 and Lys-189 and stabilizes the $\beta6$–$\beta9$ sheet, leading to a cascade of hydrogen bonds that stabilize the catalytically important DFG motif (36). (*iii*) Although Glu-170 and Tyr-330 do not make a direct contact, this residue pair allows us to monitor the C-terminal tail position relative to the catalytic loop, informing on the progress made in transitions.

We set up a periodic box ($70 \times 70 \times 70$ Å^3) to prevent ATP from flying away from the PKA. The simulations are initiated by positioning the center of a single ATP molecule $\approx$20 Å away from its target binding cleft. This initial distance of ATP from the binding pocket is large enough to randomize the orientation of PKA before it reaches the pocket. The ATP diffuses around the PKA, and $\approx$50% of them bind to the binding cleft (Fig. 2*B*), whereas the other $\approx$50% fail to bind within our maximum simulation time of 30 μs (Fig. 2*C*). In the absence of ATP in its binding cleft, the distance reporters indicate that the structure remains in an open form. The binding event of the ATP to the binding cleft is probed by using the distance between 2 atoms of the ATP [the adenyl ring (N6) and the γ-phosphorus atom (P)] and 2 residues (Ala-70 and Ser-53) of PKA. In the trajectory shown in Fig. 2*B*, the γ-phosphate of ATP

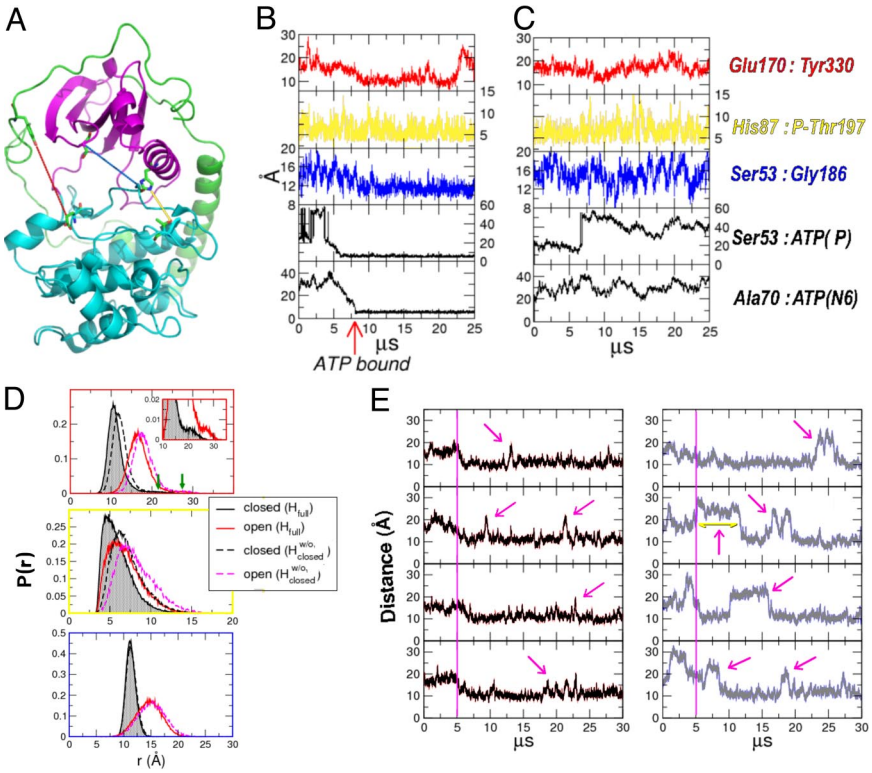

Fig. 2. Dynamics of PKA monitored through interresidue distances, r. (*A*) Colored lines are drawn between the residue pairs (red for Glu-170/Tyr-330, yellow for His-87/P-Thr-197, blue for Ser-53/Glu-186) on the PKA structure. (*B* and *C*) The $r(t)$s are shown for 2 sample trajectories. In *B*, the ATP has successfully bound to the binding pocket, whereas in *C*, the ATP has never bound to the PKA within 25 μs. The distances between γ-phosphate of ATP and Ser-53 and between the N6 nitrogen atom of ATP and Ala-70 are used for probing the ATP-binding event. The abrupt and large fluctuation in ATP position is a computational artifact due to the periodic condition used in the simulations. (*D*) Distributions of r ($P(r)$) for the reporter residue pairs are calculated from the simulations using 2 different Hamiltonians H_{full} (solid lines) and $H^{\text{w/o}}_{\text{closed}}$ (dashed lines). In the $P(r)$ of Glu-170/Tyr-330, a small hump appears at large distances (green arrows are used for markers, and the *Inset* magnifies the humps). (*E*) Dynamics of Glu-170/Tyr-330. The line in magenta at t = 5 μs indicates the moment when ATP is inserted at the binding pocket. Even after the ATP is bound to the binding pocket, the $r(t)$ value hops and makes short and long pauses at large distances. Those pauses are indicated by using the arrows. (*Left*) The typical trajectories observed among the multiple (100) trajectories are shown. (*Right*) The trajectories shown are those showing long pauses.

initially entered the binding cleft, and took ≈2–3 μs for the adenine ring to flip its orientation to bind.

Once the ATP is successfully bound (Fig. 2*B*), both interresidue distances and fluctuations diminish, which is shown more clearly [$P(r)$] the histogram of the interresidue distances before and after the ATP binding (see Fig. 2*D*). To dissect the contributions from the ATP–PKA contacts and pure closed contacts ($C \cap O^C$, see *SI Text*) to the closed conformation, we tested 2 energy Hamiltonians. One is H_{full} that uses both PKA–ATP contacts and closed contacts as driving forces to transform open state to closed state. The other is $H^{\text{w/o}}_{\text{closed}}$ that uses only PKA–ATP contacts as a driving force for open-to-closed transition (see *SI Text* for details). In both sets of simulations, we observe $P(r)$ shift toward the closed conformation upon ATP binding. It is noteworthy that the local compaction around the ATP-binding pocket is almost identical under both H_{full} and $H^{\text{w/o}}_{\text{closed}}$ when probed by using the Ser-53/Gly-186 pair (Fig. 2*D Bottom*). The distances between the residues that are not in direct contact with ATP, however, are more effectively compacted when H_{full} is used. For instance, the His-87/P-Thr-197 pair, which is important for the kinase activity, is less likely to be formed in the absence of closed contacts (Fig. 2*D Middle*). Although $H^{\text{w/o}}_{\text{closed}}$ alone can induce both the local and global compaction to some degree, a full global compaction that eventually leads to the exact functional structure is only achieved by properly incorporating the closed contacts.

Both the mean and variance of $P(r)$ decrease upon ATP binding (Fig. 2*D*). The decreased variance is related to the entropy reduction of the PKA conformation upon ATP binding; a multitude of new contacts drive the structure toward the closed conformation. If the enthalpy gain from ATP binding is smaller than the entropy reduction in residue fluctuation, the closed conformation would not be favored. We tested this simple thermodynamics by reducing the strength of ATP–PKA interactions [$\varepsilon_h(A_i,B_j)$, $\varepsilon_h(A_i,S_j)$, and $\varepsilon_l^{\text{ATP}}$ in Eq. **s3**; see *SI Text* for details] in the current model by 10-fold and found that even when ATP is inserted into the binding cleft, it dissociates spontaneously from PKA (Fig. S2). This situation is tantamount to the shift of the chemical equilibrium from PKA(C)·ATP to PKA(O) + ATP in the following reaction scheme:

$$\text{PKA(O)} + \text{ATP} \rightleftharpoons \text{PKA(C)}\cdot\text{ATP} \rightarrow \text{PKA(C)}\cdot\text{ADP}$$

$$+ \text{P}_\text{i} \xrightarrow{20s^{-1}} \text{PKA(O)} + \text{ADP}.$$

By using the time constant of ADP dissociation from PKA (≈0.05 s) (42, 43), which is the rate-limiting step for substrate phosphorylation (44), and assuming the Kramers' prefactor of ≈1 μs (45), we estimate that the free-energy barrier for ADP dissociation is ≈11 k_BT. Because ATP binds with similar affinity as ADP, ADP should not dissociate within the current simulation time (<30 μs).

Bimodal Hopping Transition Monitored by Glu-170/Tyr-330 Pair. The small humps in $P(r)$ of the Glu-170/Tyr-330 pair at both open and closed ensembles are one of the interesting findings of this study (Fig. 2*D*). To identify the origin of these small humps, we scanned all 100 trajectories produced by inserting the ATP into the binding cleft at t = 5 μs. Most of the trajectories behave as in Fig. 2*E Left*, showing an occasional transient hopping to a large distance. The trajectories (those in Fig. 2*E Right*), however, shows erratic dynamics. Even after ATP is stably bound the Glu-170/Tyr-330 pair exhibits long pauses lasting up to 7 μs at large distance values. The transitions between large and small distances are sharp. This suggests that the PKA hops between the 2 local basins of attraction in the multidimensional energy landscape. Similar behavior of first-order transition and population shift has been suggested by recent FRET experiments on the transition dynamics of adenylate kinase transition dynamics with/without ligand (3).

Kinetic Analysis Reveals the Kinetic Hierarchy. Kinetic analysis on the ensemble of time traces of $r(t)$ averaged over 100 trajectories near the binding cleft (Ser-53/Gly-196) and the one away from the binding cleft (Glu-170/Tyr-330) reveals that local dynamics is faster than global dynamics (see Fig. 3*A*). Both dynamics are analyzed by

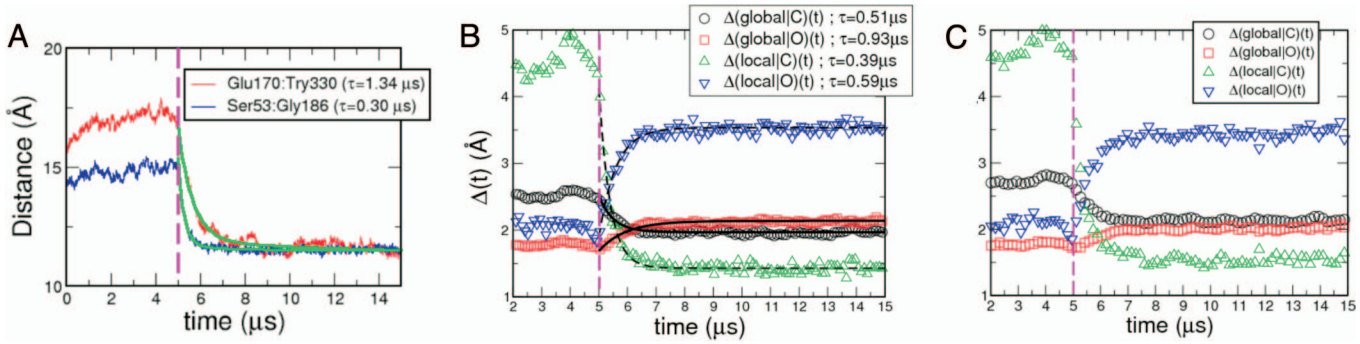

Fig. 3. Kinetic hierarchy. (*A*) Dynamics of interresidue distance. Upon ATP binding to the binding pocket at $t = 5$ μs, the average distance between Glu-170 and Tyr-330 decays biexponentially as $\approx 0.92 \times e^{-t/0.60\mu s} + 0.08 \times e^{-t/9.76\mu s}$, whereas the distance between Ser-53 and Gly-186 decays as $\approx e^{-t/0.30\mu s}$. (*B*) Ensemble dynamics monitored by using RMSD. The global and local RMSDs relative to open and closed structures are plotted with time. The local RMSD is measured with respect to Gly-rich loop. (*C*) Ensemble dynamics monitored by using RMSD in the absence of closed contacts. In this case, ATP is the only driving force for open-to-closed transitions. Although the local dynamics resulting from the direct interaction with ATP are similar to the one with closed contacts (*B*), the global dynamics are altered in the absence of the closed contacts. At steady state, $\Delta(\text{global}|C)$ reaches ≈2.5 Å (*B*), which is greater than $\Delta(\text{global}|C) \approx 2.2$ Å in the presence of closed contacts (*C*). The local interactions from ATP binding can be used to transform PKA molecules to the closed state, but the resulting structures are not as compact as those with closed native contacts included.

fitting to exponential functions. The Ser-53/Gly-196 pair kinetics fits to a single exponential with a time constant of 0.30 μs. Whereas the Glu-170/Tyr-330 pair dynamics fits to a double exponential, 92% of the molecule decays at 0.6 μs and 8% of the molecule decays an order of magnitude more slowly (≈9.8 μs). Even in the presence of ATP in its binding cleft, a stark example of the slow dynamics of the Glu-170/Tyr-330 pair is shown in Fig. 2*E Right* second tracing from the top (the regions above the yellow arrow).

The finding that local dynamics around the binding cleft is faster than the global motion of the entire PKA molecule is also confirmed by calculating the kinetics of local and global RMSD relative to the open (O) or closed (C) structure ($\Delta(t)$). The global RMSD is computed by using the whole molecule; the local RMSD is computed by using the Gly-rich loop (Fig. 3*B*). We observe that the local dynamics is faster than the global dynamics [τ(local) ≤ τ(global)] (46, 47), which strongly suggests that the signal of compaction gradually propagates from the binding pocket to the exterior region through a network of native contact pairs. The kinetic hierarchy found in the above analysis is reminiscent of the "three-shell" model (48) for the intramolecular cAMP-dependent signaling networks in the regulatory domain of PKA.

Correlated Motion of the Molecule. The elastic network model (or Gaussian network model) provides a quick grasp of the equilibrium dynamics of the protein architecture (49, 50). Fluctuation matrices $\langle \delta\vec{R}_i \cdot \delta\vec{R}_j \rangle$, as in a Gaussian network, can be calculated by using the simulated ensemble of open and closed structures.

$$\mathcal{M}_{ij}(O \text{ or } C) = \langle \delta\vec{R}_i \cdot \delta\vec{R}_j \rangle_{O \text{ or } C} \qquad [1]$$

$$= \frac{1}{N_{str}} \sum_{n=1}^{N_{str}} \Big(\sum_{\alpha=1}^{3} (x_{i,\alpha}(n) - \bar{x}_{i,\alpha})(x_{j,\alpha}(n) - \bar{x}_{j,\alpha}) \Big),$$

where $x_{i,\alpha} = x_i, y_i, z_i$ for $\alpha = 1, 2, 3$, $x_{i,\alpha} \equiv \sum_{n=1}^{N_{str}} x_{i,\alpha}(n)$, and N_{str} is the number of structures used in the numerical average. $\langle \delta\vec{R}_i \cdot \delta\vec{R}_j \rangle$ calculated in Fig. 4 shows that fluctuations of the Gly-rich loop, activation loop, and C-terminal tail are, on the average, positively correlated. The amplitude of the correlation between these regions is large for the open structure ensemble. Comparisons of the mean-square displacement for the open and the closed structure show that Gly-rich loop and C-terminal tail are the most significantly stabilized regions upon ATP binding and that the catalytic loop is also stabilized (Fig. 4*D*). Our findings are consistent with the recent experiment (2) that has identified the H/D exchange protected region in the presence of ADP; Gly-rich loop, catalytic loop, C-helix, and C-terminal tail. Interestingly, we find the enhanced fluctuations of the N-terminal tail (the end of A-helix) and of the peptide binding loop region (residues 235–240) upon ATP binding, which is amenable to a further experimental test.

PKA Transforms to the Closed Structure by Means of Cracking. We monitor the transition dynamics by using all of the backbone–backbone and side chain–side chain native contacts specified in Fig. 1 *D* and *E* (see also *SI Text* on the importance of including side chains into our model). The average fraction of native contact between i and j (Q_{ij}) is calculated over the ensemble of trajectories,

$$Q_{ij}(t) = \frac{1}{N} \sum_{k=1}^{N} \Theta(R_c^{\xi} - |\vec{r}_{i,k}(t) - \vec{r}_{j,k}(t)|), \qquad [2]$$

where N (=100) is the number of trajectories we simulated, $\vec{r}_{i,k}(t)$ refers to the position vector of ith residue at time t in kth trajectory, $\Theta(\ldots)$ is the Heaviside step function with native cutoff distance $R_c^B = 8$ Å for backbone–backbone and $R_c^S = 5$ Å for side chain–side chain native pairs. The formation of the pure closed contacts becomes more favorable when an ATP binds to the binding site. Fig. S3 shows that such additional contact formations are made at the 2 regions; one between the C-terminal tail and the linker connecting the large and small lobes (residues 120–127) and the other between the C-helix and the activation loop.

Surprising results are observed when some of the open contacts are examined. The time evolutions of Q_{ij} in Fig. 6 behave very differently from those in Fig. S3. Instead of monotonic variations of contacts, the contact pairs unfold and reassociate (*i*) at the interface formed by the C-terminal tail, the β-strands 1 and 2 and (*ii*) at the interface between the catalytic loop and the F-helix (23, 28, 51). When the ATP-binding pocket is being reorganized to interact with the ATP, the native contacts are temporarily removed ("cracking") to accommodate the interactions with the ATP. The time scales of cracking vary depending on the residue of interest. Another unexpected event is observed at the interface of β-strands 3, 4, and 5. The residue pair of (68,121) gets more associated upon ATP binding and relaxes to a smaller steady-state value [see $Q_{68,121}(t)$ and $Q_{104,120}(t)$ inside the blue box in Fig. 5]. Folded proteins are densely packed systems. The process of the insertion of an external molecule to a narrow and crowded region definitely entails nontrivial dynamics. Although proteins are also flexible to some degree to accommodate external stress, the elastic flexibility without cracking or anticracking persists only at the local basin of attraction where minor variations of structure can be tolerated (31). If proteins are

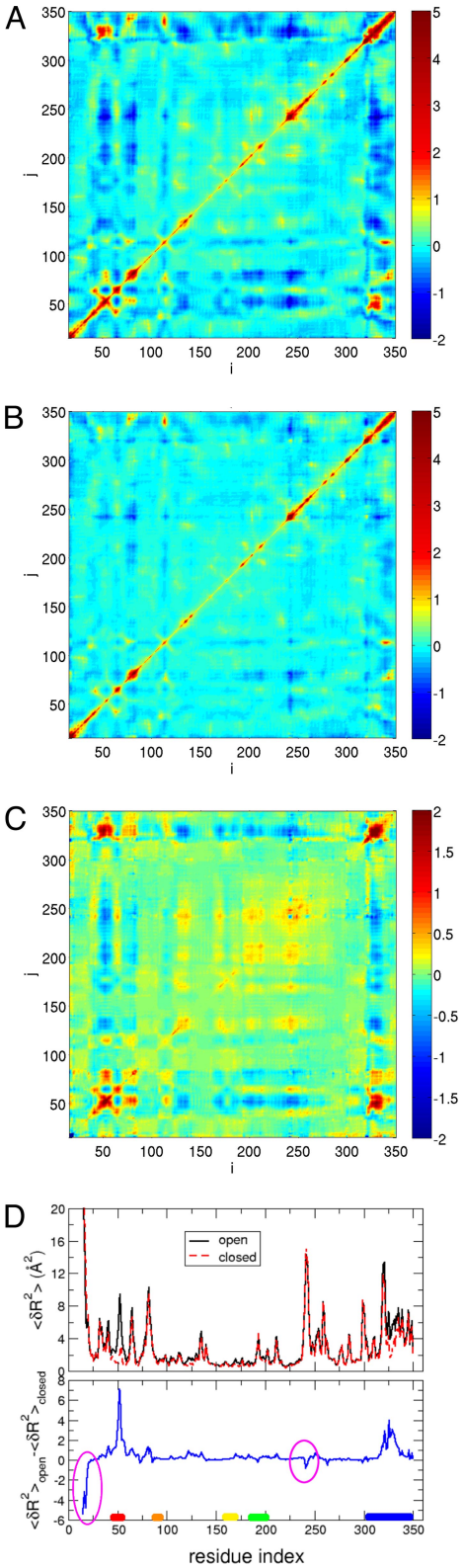

Fig. 4. Fluctuation–fluctuation correlation matrices. Open [$\mathcal{M}_{ij}$(O)] (*A*) and closed [$\mathcal{M}_{ij}$(C)] (*B*) ensembles and their difference [$\mathcal{M}_{ij}$(O) − $\mathcal{M}_{ij}$(C) (*C*). (*D*) The mean-square displacement at each residue is compared between open [$\mathcal{M}_{ii}$(O)] and closed [$\mathcal{M}_{ii}$(C)] ensembles. The sequence regions for Gly-rich loop (residues 47–58), C-helix (residues 85–97), catalytic loop (residues 166–171), activation loop (residues 184–204), and C-terminal tail (residues 301–350) are marked by using the same colors as in Fig. 1 *A*, *D*, and *E*. The sequence regions involving enhanced fluctuation upon ATP binding are enclosed in magenta circles.

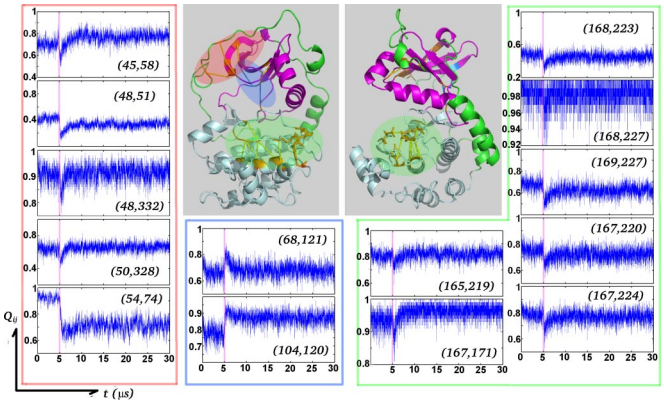

Fig. 5. Cracking dynamics of PKA upon ATP binding. Some native contact pairs partially unfold and refold when ATP binds. Average fractions of native contacts of the residue pairs undergoing cracking are calculated over 100 trajectories by using Eq. **2**. The cracking occur at the interface formed by β strands 1, 2, and C-terminal tail (regions shadowed in pale red) and at the interface between catalytic loop and F-helix (region shadowed in pale green). The residue pairs in pale blue region [residue pairs (68, 121) and (104, 120)] involve anticracking process upon ATP binding. The figure is organized similar to Fig. S3.

to make a large conformational changes beyond its elastic flexibility, it has to overcome many local barriers defined in the multidimensional energy landscape, manifesting its fragility (23, 25).

Concluding Remarks

We presented an in-depth mechanism for ligand-induced transitions in PKA. Although the multiple trajectories generated by Brownian dynamics simulations show significant heterogeneity, reflecting the multidimensional nature of the underlying energy landscape (52, 53), the overall trend gleaned from the ensemble average provides insights into the allosteric transitions.

With a conserved tertiary motif such as the hydrophobic spine (Leu-95–Leu-106–Tyr-164–Phe-185) that coordinates the catalytically competent form (36), PKA can recognize ATP by employing residues in the catalytic loop, activation loop, Mg^{2+} binding loop, and the Gly-rich loop (see Fig. 1*A*). The binding of ATP to PKA suppresses the fluctuations of the residues enveloping the binding pocket, enabling the formation of extra intramolecular contacts that are not stable in the open structure (Fig. 1*B*). Signals of local stabilization due to the ligand binding radiate outward toward the entire molecule via a network of contacts (48, 54, 55), transforming the PKA from open a closed form. During the population shift from open to closed ensemble, the local dynamics precedes the global dynamics of the entire molecule, i.e., the kinetic hierarchy is manifested.

Detailed analysis of the dynamics of residue pairs revealed that some of the secondary motifs in PKA have to partially unfold and refold for the time interval of 1-5 μs after the ligand binding, behaving as fragile objects, to accommodate the structural change. After this process, the Gly lid and the charged residues in the catalytic loop can securely hold the ligand in place (see Fig. S1*B*). The present model corroborates the previous theoretical prediction of cracking along the allosteric transition pathways (23, 28, 51). Partial local unfoldings and reformations of residue contacts are required to detour high free-energy barriers to make transitions. Such dynamics are neither simply an artifact of energy parameters nor unique to ligand-induced transitions of PKA. Rather, they are ubiquitous and can be found in the systems demonstrating the fly-casting mechanism of protein–protein interactions (25, 56) and in the large-scale movement of apical domain of GroEL in the $T \rightarrow R \rightarrow R''$ transitions (46).

Although the extent of the domain displacement studied in the PKA transition dynamics is small compared with other large-scale

allosteric transitions found in molecular motors such as kinesin (24, 25) and GroEL (46), the basic mechanism for ligand-induced transitions identified in the present study should, in principle, be applied for other larger molecular systems.

Methods

To accomplish the transition of PKA from the open to closed form upon ATP binding, we first built the energy Hamiltonian that biases the molecule to the open structure (20) (PDB ID code 1CMK) and regard the energy contributions from ATP–PKA interaction and from the native contacts of the closed structure (19) (PDB ID code 1ATP) as the perturbations to the 0th-order energy potential. If a native contact is found in both open and closed structures, we assign the equilibrium distance for the contact exclusively from the open structure (see the diagram in Fig. S4*B*). Hence, the energy contributions from the noncovalent bonds (H_{NON}) are the sum of open native contacts [$H_{NON}^{(O)}$] and pure closed native contacts [$H_{NON}^{(C\cap O^c)}$] [i.e., $H_{NON} = H_{NON}^{(O)} + H_{NON}^{(C\cap O^c)}$]. The contribution of $H_{NON}^{(C\cap O^c)}$ to the PKA compaction becomes favorable when ATP is bound to the catalytic site of PKA. The full details of energy functions and simulation methods are described in *SI Text*; (see also Movie S1).

ACKNOWLEDGMENTS. We are grateful to Dr. Alexandr P. Kornev for illuminating discussions. This work was supported by the Center for Theoretical Biological Physics sponsored by the National Science Foundation (NSF) (Grant PHY-0822283) with additional support from NSF Grant MCB-0543906. C.H. acknowledges support from the Korea Science and Engineering Foundation grant funded by the Korean Government Ministry of Science and Technology Grant R01-2008-000-10920-0) and the Korea Research Foundation Grant funded by Korean Government Grants KRF-C00142 and KRF-C00180. P.A.J. is supported by National Institutes of Health Grant DK-054441.

1. Pauling L (1948) Nature of forces between large molecules of biological interest. *Nature* 161:707–709.
2. Andersen MD, Shaffer J, Jennings PA, Adams JA (2001) Structural characterization of protein kinase A as a function of nucleotide binding-hydrogen–deuterium exchange studies using matrix-assisted laser desorption ionization-time of flight mass spectrometry detection. *J Biol Chem* 276:14204–14211.
3. Hanson JA, *et al.* (2007) Illuminating the mechanistic roles of enzyme conformational dynamics. *Proc Natl Acad Sci USA* 104:18055–18060.
4. Tang C, Schwieters CD, Clore GM (2007) Open-to-closed transition in apo maltose-binding protein observed by paramagnetic NMR. *Nature* 449:1078–1082.
5. Trewhella J (1997) Insights into biomolecular function from small-angle scattering. *Curr Opin Struct Biol* 7:702–708.
6. Kay LE (1998) Protein dynamics from NMR. *Biochem Cell Biol* 76:145–152.
7. Woods VL, Jr, Hamuro Y (2001) High resolution, high-throughput amide deuterium exchange-mass spectrometry (DXMS) determination of protein binding site structure and dynamics: Utility in pharmaceutical design. *J Cell Biochem* Suppl 89–98.
8. Fontana A, *et al.* (2004) Probing protein structure by limited proteolysis. *Acta Biochim Pol* 51:299–321.
9. Cheng X, Shaltiel S, Taylor SS (1998) Mapping substrate-induced conformational changes in cAMP-dependent protein kinase by protein footprinting. *Biochemistry* 37:14005–14013.
10. Hamuro Y, *et al.* (2002) Phosphorylation driven motions in the COOH-terminal Src kinase, Csk, revealed through enhanced hydrogen–deuterium exchange and mass spectrometry (DXMS). *J Mol Biol* 76:145–152.
11. Lee T, Hoofnagle AN, Resing KA, Ahn NG (2005) Hydrogen exchange solvent protection by an ATP analogue reveals conformational changes in ERK2 upon activation. *J Mol Biol* 353:600–612.
12. Krebs EG, Fischer EH (1956) Ther phosphorylase-B to phosphorylase-A converting enzyme of rabbit skeletal muscle. *Biochim Biophys Acta* 20:150–157.
13. Taylor SS, *et al.* (1993) A template for the protein kinase family. *Trends Biochem Sci* 18:84–89.
14. Levinson NM, Seeliger MA, Cole PA, Kuriyan J (2008) Structural basis for the recognition of c-Src by its inactivator Csk. *Cell* 134:124–134.
15. Burak WR, Shaw AS (2000) Signal transduction: Hanging on a scaffold. *Curr Opin Cell Biol* 12:211–216.
16. Cowan-Jacob SW, *et al.* (2005) The crystal structure of a c-Src complex in an active conformation suggests possible steps in c-Src activation. *Structure (London)* 13:861–871.
17. Xu W, Doshi A, Lei M, Eck MJ, Harrison SC (1999) Crystal structures of c-Src reveal features of its autoinhibitory mechanism. *Mol Cell* 3:629–638.
18. Taylor SS, *et al.* (2004) PKA: A portrait of protein kinase dynamics. *Biochim Biophys Acta* 1697:259–269.
19. Knighton DR, *et al.* (1993) 2.0 Å refined crystal structure of the catalytic subunit of cAMP-dependent protein kinase complexed with a peptide inhibitor and detergent. *Acta Crystallogr* D 49:357–361.
20. Zheng J, Knighton DR, Xuong N, Taylor SS, Sowadski JM (1993) Crystal structures of the myristylated catalytic subunit of cAMP-dependent protein kinase reveal open and closed conformations. *Protein Sci* 2:1559–1573, 1993.
21. Johnson DA, Akamine P, Radzio-Andzeim, E., Madhusudan, Taylor SS (2001) Dynamics of cAMP-dependent protein kinase. *Chem Rev* 101:2243–2270.
22. Koshland DE (1958) Application of a theory of enzyme specificity to protein synthesis. *Proc Natl Acad Sci USA* 44:98–104.
23. Miyashita O, Onuchic JN, Wolynes PG (2003) Nonlinear elasticity, protein quakes, and the energy landscapes of functional transitions in proteins. *Proc Natl Acad Sci USA* 100:12570–12575.
24. Hyeon C, Onuchic JN (2007) Internal strain regulates the nucleotide binding site of the kinesin leading head. *Proc Natl Acad Sci USA* 104:2175–2180.
25. Hyeon C, Onuchic JN (2007) Mechanical control of the directional stepping dynamics of the kinesin motor. *Proc Natl Acad Sci USA* 104:17382–17387.
26. Adams JA, Talyor SS (1992) Energetic limits of phosphotransfer in the catalytic subunit of cAMP-dependent protein kinase as measured by viscocity experiments. *Biochemistry* 31:8516–8522.
27. Zhou J, Adams JA (1997) Participation of ADP dissociation in the rate-determining step in cAMP-dependent protein kinase. *Biochemistry* 36:15733–15738.
28. Whitford PC, Miyashita O, Levy Y, Onuchic JN (2007) Conformational transitions of adenylate kinase: Switching by cracking. *J Mol Biol* 366:1661–1671.
29. Arora K, Brooks CL, III (2007) Large-scale allosteric conformational transitions of adenylate kinase appear to involve a population-shift mechanism. *Proc Natl Acad Sci USA* 104:18496–18501.
30. Lou H, Cukier RI (2006) Molecular dynamics of apo-adenylate kinase: A principal component analysis. *J Phys Chem B* 110:12796).
31. Henzler-Wildman KA, *et al.* (2007) A hierarchy of timescales in protein dynamics is linked to enzyme catalysis. *Nature* 450:913–916.
32. Faraldo-Gomez JD, Roux B (2007) On the importance of a funneled energy landscape for the assembly and regulation of multidomain Src tyrosin kinase. *Proc Natl Acad Sci USA* 104:13643–13648.
33. Yang S, Roux B (2008) Src kinase conformational activation: Thermodynamics, pathways, and mechanisms. *PLoS Comput Biol* 4:e1000047.
34. Levinson NM, *et al.* (2006) A Src-like inactive conformation in the Abl tyrosin kinase domain. *PLoS Biol* 4:e144.
35. Berteotti A, *et al.* (2009) Protein conformational transitions: The closure mechanism of a kinase explored by atomistic simulations. *J Am Chem Soc* 131:244–250.
36. Kornev AP, Haste NM, Taylor SS, Ten Eyck LF (2006) Surface comparison of active and inactive protein kinases identifies a conserved activation mechanism. *Proc Natl Acad Sci USA* 103:17783–17788.
37. Steinberg RA, Cauthron RD, Symcox MM, Shuntoh H (1993) Autoactivation of catalytic (Cα) subunit of cyclic AMP-dependent protein kinase by phosphorylation of threonine 197. *Mol Cell Biol* 13:2332–2341.
38. Adams JA, McGlone ML, Gibson R, Taylor SS (1995) Phosphorylation modulates catalytic function and regulation in the cAMP-dependent protein kinase. *Biochemistry* 34:2447–2454.
39. Jeffrey PD *et al.* (1995) Mechanism of CDK activation revealed by the structure of a cyclinA-CDK2 complex. *Nature* 376:313–320.
40. Canagarajah BJ, Khokhlatchev A, Cobb MH, Goldsmith EJ (1997) Activation mechanism of the MAP kinase ERK2 by dual phosphorylation. *Cell* 90:859–869.
41. Cheng X, Ma Y, Moore M, Hemmings BA, Taylor SS (1998) Phosphorylation and activation of cAMP-dependent protein kinase by phosphoinositide-dependent protein kinase. *Proc Natl Acad Sci USA* 95:9849–9854.
42. Grant BD, Adams JA (1996) Pre-steady-state kinetic analysis of camp-dependent protein kinase using rapid quench flow techniques. *Biochemistry* 35:2022–2029.
43. Adams JA (2002) Activation loop phosphorylation and catalysis in protein kinases: Is there functional evidence for the autoinhibitor model? *Biochemistry* 42:601–607.
44. Lu B, Wong CF, McCammon JA (2005) Release of ADP from the catalytic subunit of protein kinase A: A molecular dynamics simulation study. *Protein Sci* 14:159–168.
45. Kubelka J, Hofrichter J, Eaton WA (2004) The protein folding 'speed limit'. *Curr Opin Struct Biol* 14:76–88.
46. Hyeon C, Lorimer GH, Thirumalai D (2006) Dynamics of allosteric transition in GroEL. *Proc Natl Acad Sci USA* 103:18939–18944.
47. Chen J, Dima RI, Thirumalai D (2007) Allosteric communication in dihydrofolate reductase: signaling network and pathways for closed to occluded transition and back. *J Mol Biol* 374:250–266.
48. Das R, *et al.* (2007) cAMP activation of PKA defines an ancient signaling mechanism. *Proc Natl Acad Sci USA* 104:93–98.
49. Maragakis P, Karplus M (2005) Large amplitude conformational change in proteins explored with a plastic network model: Adenylate kinase. *J Mol Biol* 352:807–822.
50. Haliloglu T, Bahar I, Erman B (1997) Gaussian dynamics of folded proteins. *Phys Rev Lett* 79:3090–3093.
51. Onuchic JN, Kobayashi C, Miyashita O, Jennings P, Baldridge KK (2006) Exploring biomolecular machines: Energy landscape control of biological reactions. *Philos Trans R Soc London Ser B* 361:1439–1443.
52. Onuchic J, Luthey-Schulten Z, Wolynes PG (1997) Theory of protein folding: The energy landscape perspective. *Annu Rev Phys Chem* 48:539–600, 1997.
53. Thirumalai D, Hyeon C (2005) RNA and protein folding: Common themes and variations. *Biochemistry* 44:4957–4970.
54. Zheng W, Brooks BR, Doniach S, Thirumalai D (2005) Network of dynamically important residues in the open/closed transition in polymerases is strongly conserved. *Structure (London)* 13:565–577.
55. Kornev AP, Taylor SS, Ten Eyck LF (2008) A generalized allosteric mechanism for *cis*-regulated cyclic nucleotide binding domains. *PLoS Comp Biol* 4:1–9.
56. Shoemaker BA, Portman JJ, Wolynes PG (2000) Speeding molecular recognition by using the folding funnel: The fly-casting mechanism. *Proc Natl Acad Sci USA* 97:8868–8873.